

# An Improved Active Disturbance Rejection Control for Bode's Ideal Transfer Function

Bolin Li, and Lijun Zhu

**Abstract**—This paper presents an active disturbance rejection control (ADRC) scheme with an improved fractional-order extended state observer (IFO-ESO). Based on the new ADRC scheme, the open-loop transfer function of a high-order system can be approximately rendered to a so-called Weighed Bode's ideal transfer function, whose closed-loop performance is less prone to the controller parameter variations. The design of the IFO-ESO helps reduce the number of system states to be estimated and improves the performance of closed-loop system over the fractional-order active disturbance rejection control (FO-ADRC) in the literature. Compared with the integer-order active disturbance rejection controller (IO-ADRC) and FO-ADRC, the auxiliary tracking controller of IFO-ADRC has a simpler form. Frequency-domain analysis shows that IFO-ESO has better estimation performance than typical fractional-order ESO (FO-ESO), and time-domain simulation demonstrates that the proposed ADRC has better transient performance and is more robust against the parameter variations than FO-ADRC and IO-ADRC. The proposed ADRC is applied to permanent magnet synchronous motor (PMSM) servo control system and demonstrates its capability in a real-world application.

## I. INTRODUCTION

Fractional calculus has been applied for the controller design in the fields of permanent magnet synchronous motor gas-turbine and heating-furnace etc., to improve the system performance in recent years [1], [2], [3]. Many fractional-order controllers have been proposed, including fractional-order sliding mode controller [4], intelligent PID controller [5], PID controller [6], active disturbance rejection controller [7], and so on.

In 1940s, Bode [8] suggested an ideal open-loop transfer function, called Bode's ideal transfer function (BITF). An advantage of the BITF is that when the open-loop gain varies, the gain crossover frequency will change while the phase margin remains the same. Due to this characteristic, BITF has been used as the reference model to design the fractional-order controller [9], [10], [11]. Using the BITF method, the closed-loop system achieve the iso-damping property (the phase derivative with respect to the frequency is zero) and the overshoots of the step responses will remain almost constant even when the open-loop gain varies. The controller design is straightforward for low-order systems by using BITF method [12], [13], [14], but becomes complicated for high-order systems [15], in particular with uncertainties.

The integer-order active disturbance rejection control (IO-ADRC) proposed by Gao [16] provides a strategy for control system design with uncertainties. The core idea of IO-ADRC is to improve the robustness of the system using extended state observer (IO-ESO, or extended high-gain observer) [17], [18]

to estimate the total disturbances, including internal disturbance caused by system uncertainties and external disturbance [19], [20]. Inspired by the ADRC structure, a fractional-order ADRC (FO-ADRC) was proposed in [15], and approximately converted a class of integer-order systems into a weighted Bode's ideal transfer function (WBITF). WBITF is a higher-order transfer function and can be approximated to a BITF in the low-frequency band.

This paper is along the research line of proposing a new type of fractional-order ESO structure and then an improved fractional-order ADRC (IFO-ADRC) to achieve a WBITF. The main contributions of the paper can be summarized as follows. First, a new type of ESO, called IFO-ESO, is proposed to compensate for the system uncertainties and external disturbance. In comparison to [15], less state is estimated in the IFO-ESO and high-order dynamics are not included in the extended state, which potentially improves the disturbance estimation performance of IFO-ESO over FO-ESO, making the system more robust to system uncertainties and external disturbances. Better estimation performance of IFO-ESO ensures that the open-loop transfer function can be more accurately approximated into a newly introduced WBITF. With proposed IFO-ESO, the auxiliary tracking controller of IFO-ADRC also has a simpler form. Second, the stability criteria of the IFO-ESO and the IFO-ADRC closed-loop system are given. For a second-order system, we prove that when the observer gains are selected to be sufficiently large, the closed-loop system is BIBO stable.

The rest of the paper is organized as follows. Some preliminaries on fractional operator and BITF are provided and the problem is formulated in Section II. The structures of IFO-ADRC, and the BIBO stability criteria for the IFO-ESO and the closed-loop system are given in Section III. The performance analysis of the IFO-ESO in the frequency-domain is shown in Section IV. Section V presents the time-domain simulation results, followed by the experimental results on PMSM servo system in Section VI. The paper is concluded in Section VII.

## II. PRELIMINARIES AND PROBLEM FORMULATION

### A. Bode's Ideal Transfer Function

The mathematical form of Bode's ideal transfer function [8] is

$$L_o(s) = \left(\frac{\omega_g}{s}\right)^\chi \quad (1)$$

where  $\omega_g$  is the gain crossover frequency and  $\chi$  is a real-number order. In Bode plot, the slope of the magnitude curve of BITF is  $-20\chi$  dB/deg, and the phase curve is a horizontal

line at  $\chi\pi/2$  rad, both parameterized by  $\chi$ . An advantage of the BITF is that when the open-loop gain varies, the crossover frequency  $\omega_g$  will change while the phase margin constant  $\pi(1 - \chi/2)$  rad remains the same. When  $1 < \chi < 2$ , the step response of the unit negative feedback system of a BITF is similar to that of an under-damped second-order system. Due to this characteristic, the BITF has been adopted as the reference model for the controller design, particularly for low-order systems. However, converting a higher-order system into a BITF in (1) requires an irrational compensator, and is not feasible in practice. In [15], a so-called weighted BITF (WBIF) was then proposed as the series combination of the BITF and  $k$  low-pass filters, for  $1 < \chi < 2$ ,

$$L_{ol}(s) = \frac{\omega_g^\chi}{s^\chi(Ts + 1)^\kappa} \quad (2)$$

where  $\kappa$  is a positive integer satisfying  $\kappa + \chi = m$  and  $m$  represents the maximum order of the plant, and  $T$  is the time constant of the filter. Note that when  $T$  is much less than  $\omega_g$ , the characteristic of (2) is similar to that of BITF in (1). An FO-ADRC was then constructed to convert an high-order system into a WBIF with the same order.

### B. Problem Formulation

In this paper, we consider a high-order linear system as follows

$$G(s) = \frac{Y(s)}{U(s)} = \frac{b}{s^m + \sum_{i=1}^{m-1} a_i s^i + a_0} \quad (3)$$

where  $s$  is Laplace operator,  $a_i$ ,  $a_0$  and  $b$  are real numbers,  $m$  and  $i$  are positive integers with  $m$  representing the maximum order of the system. The differential equation form of system (3) with the external disturbance, denoted by  $d$ , is

$$y^{(m)} = - \sum_{i=1}^{m-1} a_i y^{(i)} - a_0 y + bu + d \quad (4)$$

The aim of this paper is first to propose an improved FO-ESO based on which the system is approximately converted (3) into a newly introduced WBIF as follows

$$G_{ol}(s) = \frac{\omega_g^\chi}{s^\chi(Ts^\gamma + 1)^\kappa} \quad (5)$$

where  $\gamma$  is the order of the fractional-order filter,  $0 < \gamma < 2$ , and  $\chi + \kappa\gamma = m$ . WBIF (5) is composed of a BITF and  $\kappa$  low-pass filters in series with the order  $\gamma$  to be specified. When  $\gamma = 1$ , WBIF (5) coincides with WBIF (2). In next section, the new WBIF with fractional-order  $\gamma$  facilitates the IFO-ESO to be proposed in next section.

The second aim of this paper is to design  $u$  such that the system output tracks a sufficiently smooth reference trajectory  $r$  and the ultimate tracking error stays in the neighborhood of the origin, i.e.,  $\lim_{t \rightarrow \infty} \|y(t) - r(t)\| < \epsilon$ , when the reference signal and its derivatives, i.e.,  $r, \dot{r}, \ddot{r}, \dots, r^{(m-1)}, r^{(m)}$  are bounded.

### C. Definitions on Fractional Operator

There are various definitions of fractional derivative [21], such as the Grunwald–Letnikov, Riemann–Liouville, Caputo definitions, and so on. The Grunwald–Letnikov (GL) is one of the most commonly used definition and adopted in this paper, whose notation is given as [22]

$${}_a D_t^\gamma f(t) = \lim_{h \rightarrow 0} \frac{1}{h^\gamma} \sum_{j=0}^{\lceil \frac{t-a}{h} \rceil} (-1)^j \binom{n_0}{j} f(t - jh) \quad (6)$$

where  $n_0$  is an integer satisfying  $n_0 - 1 < \gamma < n_0$  and  $\gamma$  is a fractional order,  $h$  and  $\lceil \frac{t-a}{h} \rceil$  are time increment and integer part of the upper limit of summation, respectively.

The binomial coefficient is  $\binom{n_0}{j} = \frac{\Gamma(n_0+1)}{\Gamma(j+1)\Gamma(n_0-j+1)}$  where  $\Gamma(\bullet)$  is Euler's gammafunction. The Laplace transform of the GL fractional-order derivative with zero initial condition is given as  $\mathcal{L}\{{}_a D_t^\gamma f(t)\} = s^\gamma F(s)$ .

## III. IMPROVED ACTIVE DISTURBANCE REJECTION CONTROLS

### A. Structures of IFO-ESO and IFO-ADRC

In this section, we will use IFO-ESO and IFO-ADRC to approximately convert the system (3) into a WBIF (5). Equation (4) can be rewritten as follows,

$$y^{(m)} = f_{ifo}(y^{(1)}, y^{(2)}, \dots, y^{(m-1)}, y, u, t) + b_0 u \quad (7)$$

where  $f_{ifo} = - \sum_{i=1}^{m-1} a_i y^{(i)} - a_0 y + (b - b_0)u + d$ . Note that  $f_{ifo}$  can be regarded as the total disturbance where the term  $- \sum_{i=1}^{m-1} a_i y^{(i)} - a_0 y + (b - b_0)u$  is the internal disturbance due to uncertain parameters and  $d$  is the external disturbance.

Let  $\chi$  be a fractional number satisfying  $1 < \chi < 2$ ,  $n = \lceil \frac{m}{\chi} \rceil + 1$ ,  $\gamma = \frac{m-\chi}{n-1}$ , and  $\gamma < \nu < \chi$ . Note  $x_1 = y, x_2 = y^{(\chi)}, x_3 = y^{(\gamma+\chi)}, \dots, x_n = y^{((n-2)\gamma+\chi)}, x_{n+1} = f_{ifo}^{(\nu)}(y^{(1)}, y^{(2)}, \dots, y^{(m-1)}, y, u, t)$  where  $x_1, x_2, \dots, x_n$  represent system states and  $x_{n+1}$  is an extended state. Let  $x = [x_1, x_2, \dots, x_n, x_{n+1}]^T$ . The state-space representation of (7) is given as follows

$$\begin{aligned} {}_a D_t^q x &= Ax + Bu + E h_{ifo} \\ y &= Cx \end{aligned} \quad (8)$$

where  $q = [\chi, \gamma, \dots, \gamma, \nu]^T$  and

$$\begin{aligned} A &= \begin{bmatrix} 0_{n \times 1} & I_n \\ 0 & 0_{1 \times n} \end{bmatrix}, B = [0, 0, \dots, b_0, 0]^T, \\ C &= [1, 0, \dots, 0, 0], E = [0 \quad \dots \quad 0 \quad 1]^T. \end{aligned} \quad (9)$$

Then, IFO-ESO is designed to estimate  $x$  as follows

$$\begin{aligned} {}_a D_t^q z &= Az + Bu + L(y - \hat{y}) \\ \hat{y} &= Cz \end{aligned} \quad (10)$$

where  $z = [z_1, z_2, \dots, z_n, z_{n+1}]^T$  and

$$L = [\beta_1, \beta_2, \dots, \beta_n, \beta_{n+1}]^T \quad (11)$$

Note that  $L$  are extended state observer gains,  $z$  is the estimation of the state  $x$  and  $b_0$  is the nominal value of  $b$ .

The controller is designed as follows

$$u = \frac{u_0 - \hat{f}_{ifo}}{b_0} \quad (12)$$

where  $\hat{f}_{ifo} = z_{n+1}$  and  $u_0$  is auxiliary tracking controller to be designed. Then, the closed-loop system composed of (7) and (12) becomes

$$y^{(m)} = u_0 + (f_{ifo} - \hat{f}_{ifo}). \quad (13)$$

The tracking task can be fulfilled with the auxiliary tracking controller  $u_0$  in (12), designed as follows,

$$u_0 = k_p e_0 - K_0 z + K_1 \hat{r} \quad (14)$$

where  $e_0 = r - z_1$ ,  $\hat{r} = [r_1, r_2, \dots, r_n, r_{n+1}]$  with  $r_1 = r$ ,  $r_i = r^{(\chi+(i-2)\gamma)}$  for  $i = 2, 3, \dots, n+1$ . Note that  $r$  is the reference input of the closed-loop system. In particular, we choose the controller gain as  $K_0 = [0, k_{d_1}, \dots, k_{d_{n-1}}, 0]$  with  $k_{d_i} = C_{n-1}^i \omega_c^{n-1-i}$  for  $i = 1, 2, \dots, n-1$  and  $K_1 = [0, k_{d_1}, \dots, k_{d_{n-1}}, 1]$ . Substituting (14) into (13) gives

$$y^{((n-1)\gamma+\chi)} + K_0 x = k_p e_0 + K_0(x - z) + (f_{ifo} - \hat{f}_{ifo}) + K_1 \hat{r} \quad (15)$$

where we note  $m = (n-1)\gamma + \chi$ . The structure of the IFO-ADRC for a second-order plant with  $\dot{r} = 0$  and  $\ddot{r} = 0$ , is illustrated in Fig. 1.

Now, let us consider the open-loop transfer function of the IFO-ADRC and without loss of generality assume  $r \equiv 0$ . If signals  $f_{ifo}$  and  $x$  are well estimated by  $\hat{f}_{ifo}$  and  $z$ , respectively, i.e.,  $\hat{f}_{ifo} \approx f_{ifo}$  and  $z \approx x$ , the Laplace transform of the both side of (15) (with  $r \equiv 0$ ) gives

$$\frac{Y(s)}{E_0(s)} \approx k_p \frac{\frac{1}{\omega_c^{n-1}}}{s^\chi (\frac{1}{\omega_c} s^\gamma + 1)^{n-1}} \quad (16)$$

where  $Y(s)$  and  $E_0(s)$  are the Laplace transforms of  $y$  and  $e_0$ , respectively. The open-loop transfer function of the IFO-ADRC system is

$$\begin{aligned} G_{ifo}(s) &= \frac{Z_1(s)}{E_0(s)} = \frac{Z_1(s)}{Y(s)} \frac{Y(s)}{E_0(s)} \\ &\approx \bar{G}_{ifo}(s) = k_p \frac{\frac{1}{\omega_c^{n-1}}}{s^\chi (\frac{1}{\omega_c} s^\gamma + 1)^{n-1}} \end{aligned} \quad (17)$$

where  $Z_1(s)$  is the Laplace transform of  $z_1$ . Letting  $k_p = w_g^\chi \omega_c^{n-1}$  makes the approximation  $\bar{G}_{ifo}(s)$  as

$$\bar{G}_{ifo}(s) = \frac{w_g^\chi}{s^\chi (Ts^\gamma + 1)^{n-1}} \quad (18)$$

which is a WBTF in (5) with  $\kappa = n-1$  and  $T = \frac{1}{\omega_c}$ . On the one hand, due to the existence of  $n-1$  low-pass filter  $1/(Ts^\gamma+1)$ ,  $\bar{G}_{ifo}(s)$  behaves like a BITF in the low-frequency band. On the other hand, for a larger  $\omega_c$ , the approximate open-loop transfer function  $\bar{G}_{ifo}(s)$  behaves more like a BITF.

The design principle of the IFO-ADRC is summarized as follows. First, the IFO-ESO is proposed and used to construct

the controller (12) to approximately convert the original uncertain plant into a cascade integer-order integrator in (13). Then, a tracking controller (14) is proposed to approximately shape the open-loop transfer function as a WBTF.

On the contrary, the high-order term  $y^{(m)}$  is included in the total disturbance for FO-ADRC in [15] and further estimated by a higher-order ESO. As shown in Section IV, such a design of ESO has worse estimation performance. Moreover, less number of observer states and auxiliary tracking controller parameters can be used to achieve stable IFO-ADRC than FO-ADRC and IO-ADRC systems as demonstrated in Section V.

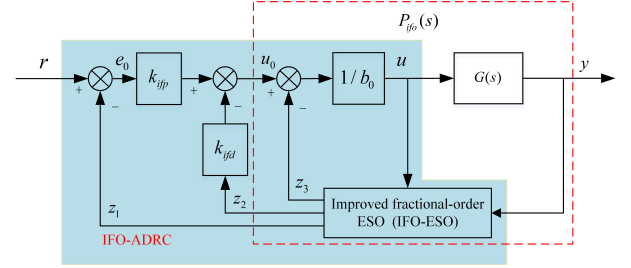


Fig. 1. Structure of the IFO-ADRC for a second-order plant.

## B. Stability Analysis of IFO-ADRC

In this section, the stability criteria for the ESO and the IFO-ADRC system are provided. Let the observer error be  $e = x - z$ . From (8) and (10), the equation of the extended state observer error can be written as

$${}_0^C D_t^\alpha e = Ae - Le_1 + Eh_{ifo}. \quad (19)$$

The characteristic polynomial of the system (19) can be obtained [23]:

$$\lambda(s) = s^{(n-1)\gamma+\chi+\nu} + \sum_{i=1}^n \beta_i s^{(n-1)\gamma+\nu} + \beta_{n+1} \quad (20)$$

Then, Theorem 3.1 will present the bounded-input bounded-output (BIBO) stability of the error system (19), when  $h_{ifo}$  is bounded. Theorem 3.2 gives the BIBO condition for the closed-loop system using characteristic equation method. A special case when  $m = n = 2$  is elaborated in Theorem 3.3, showing that when the observer gain is sufficiently large, the closed-loop system is BIBO. The proofs of Theorem 3.1 and 3.3 are given in the Appendix.

**Theorem 3.1:** Consider the error dynamics of IFO-ESO (19). Let  $\omega_0 > 1$  and  $\beta_i = C_{n+1}^i \omega_0^i$  for  $i = 1, 2, \dots, n+1$ . If  $h_{ifo}$  is bounded, then the IFO-ESO is BIBO stable, regarding  $h_{ifo}$  as the input and  $e_1$  as the output. ■

**Theorem 3.2:** Consider the IFO-ADRC closed-loop system composed of (4), (12) and (14). Let  $(p_1, q_1)$ ,  $(p_2, q_2)$

and  $(p_3, q_3)$  be pairs of coprime positive integers satisfying  $\chi = \frac{p_1}{q_1}$ ,  $\gamma = \frac{p_2}{q_2}$ , and  $\nu = \frac{p_3}{q_3}$ . Define a polynomial

$$\begin{aligned} P(w) = & (w^{p_1 q_2 q_3} (w^{(n-1) q_1 p_2 q_3} + \sum_{i=1}^{n-1} k_{d_i} w^{(i-1) q_1 p_2 q_3}) + k_p) \\ & \times (w^{(n-1) q_1 p_2 q_3 + q_1 q_2 p_3 + p_1 q_2 q_3} + \sum_{i=1}^n \beta_i w^{(n-i) q_1 p_2 q_3 + q_1 q_2 p_3} \\ & + \beta_{n+1}) + (k_p + \sum_{i=1}^{n-1} k_{d_i} (w^{p_1 q_2 q_3 + (i-1) q_1 p_2 q_3} \\ & + \sum_{j=1}^{i-1} \beta_j w^{j q_1 p_2 q_3} + \beta_i)) + (w^{p_1 q_2 q_3 + (n-1) q_1 p_2 q_3} \\ & + \sum_{j=1}^{n-1} \beta_j w^{j q_1 p_2 q_3} + \beta_n)) \times (w^{q_1 q_2 p_3} \sum_{i=0}^{m-1} a_i w^{i q_1 q_2 p_3}) \quad (21) \end{aligned}$$

Let  $\lambda = \frac{1}{q_1 q_2 q_3}$  and  $w_i$  be the  $i$ th root of the equation (21) for  $i = 1, \dots, 2mp_1 p_2 p_3 + q_1 q_2 p_3$ . If  $b = b_0$ ,  $k_p, k_{d_1}, \dots, k_{d_{m-2}}$  and  $\beta_1, \dots, \beta_{n+1}$  are selected such that all the roots satisfy  $|\arg(w_i)| > \frac{\lambda\pi}{2}$ , then the IFO-ADRC closed-loop system is BIBO stable, regarding  $d$  as the input, and  $r - y$  as the output. Moreover, the tracking error  $r(t) - y(t)$  converges to a small neighborhood of the origin as  $t \rightarrow \infty$ . ■

**Theorem 3.3:** Consider the IFO-ADRC closed-loop system composed of (4), (12) and (14) with  $m = n = 2$ . Suppose the plant (4) is stable or marginally stable, i.e.,  $a_1 \geq 0$  and  $a_0 \geq 0$ . Let  $\beta_i = C_{n+1}^i \omega_0^i$  for  $i = 1, 2, 3$ ,  $k_p > 0$ ,  $k_{d_1} > 8$ , and  $\gamma < \nu < 1$ . Then, there always exists a constant  $\omega_0 > 0$ , such that the closed-loop system is BIBO stable. Moreover, the tracking error  $r(t) - y(t)$  converges to a small neighborhood of the origin as  $t \rightarrow \infty$ . ■

#### IV. PERFORMANCE ANALYSIS OF IFO-ESO IN FREQUENCY-DOMAIN

In this section, we will compare the performance of the IFO-ESO proposed in Section III with the FO-ESO proposed in [15], whose structure for second-order plant is illustrated in Fig. 6. Note that the role of the ESO in the framework of ADRC is to estimate the uncertain dynamics and external disturbances to improve the robustness of the system. If the IFO-ESO can perfectly estimate  $\hat{f}_{ifo}$ , the IFO-ADRC can convert the original system into a cascaded integer-order integrator  $1/s^m$  in (13). Similarly, the FO-ADRC can convert the original system into a fractional-order system  $1/s^{m+\chi-1}$  (also looking from  $u_0$  to  $y$ ). Therefore, we are motivated to use the model difference between  $Y(s)/U_0(s)$  and the ideal model ( $1/s^m$  with IFO-ESO;  $1/s^{m+\chi-1}$  with FO-ESO) to assess the performance of the two ESOs. We adopt mean square error between  $Y(s)/U_0(s)$  and the ideal model in the frequency-domain to evaluate how difference the two models are. The mean square error (MSE) of two linear models is defined as

$$\begin{aligned} \text{IFO-ESO: } \Delta_{ifo}(\omega) &= 1 - (j\omega)^m P_{ifo}(j\omega) \\ \text{FO-ESO: } \Delta_{fo}(\omega) &= 1 - (j\omega)^{m+\chi-1} P_{fo}(j\omega) \quad (22) \end{aligned}$$

where  $P_{ifo}(s)$  and  $P_{fo}(s)$  are transfer function from  $u_0$  to  $y$  for IFO-ESO and FO-ESO, respectively. The MSE was used in [24] for the model identification where the problem is re-casted into an optimal problem of minimizing the model difference between the identified and ideal model in terms of the MSE. Therefore, the MSE can be used to evaluate model difference in the frequency-domain.

As in [15], for simplicity, we consider the second-order system

$$G(s) = \frac{Y(s)}{U(s)} = \frac{b}{s^2 + a_1 s + a_0}, \quad (23)$$

where the external disturbance and system uncertainty are not considered. For the fair comparison, we choose the observer gains  $\beta_1 = 3\omega_0$ ,  $\beta_2 = 3\omega_0^2$ ,  $\beta_3 = \omega_0^3$  for IFO-ESO and  $\beta_1 = 4\omega_0$ ,  $\beta_2 = 6\omega_0^2$ ,  $\beta_3 = 4\omega_0^3$ ,  $\beta_4 = \omega_0^4$  for FO-ESO with  $\omega_0 = 500$ . The system parameters are  $b = 5$ ,  $a_0 = 10$ ,  $a_1 = 10$ . Let  $\chi = 1.2$  for FO-ESO,  $\nu = 0.8$ , and  $\gamma = 0.8$  for IFO-ESO.

The Bode plot of  $P_{ifo}(j\omega)$  and  $P_{fo}(j\omega)$  are illustrated in Fig. 2 and Fig. 3, respectively. It shows that the amplitude and the phase plot of  $P_{ifo}(j\omega)$  are close to that of the ideal model within a larger frequency band than that of  $P_{fo}(j\omega)$ . In particular, the approximation of  $P_{fo}$  to  $1/s^{2.2}$  gets worse in high-frequency band. It can be inferred that the IFO-ESO has better performance in terms of disturbance estimation than the FO-ESO. Fig. 4 and Fig. 5 show the curves of the mean-square

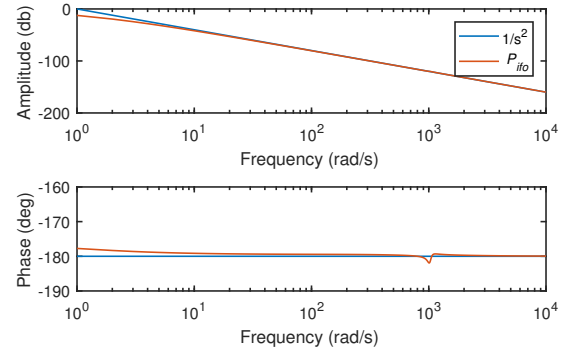


Fig. 2. Bode plot of  $P_{ifo}(j\omega)$  for IFO-ESO.

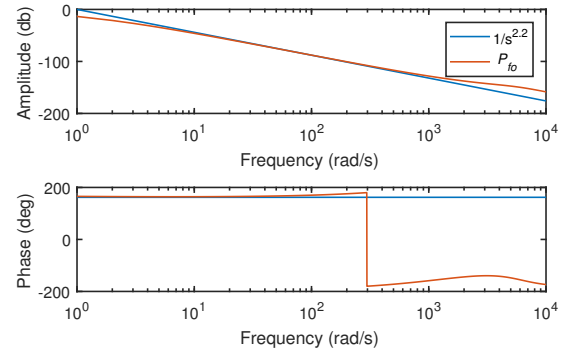


Fig. 3. Bode plot of  $P_{fo}(j\omega)$  for FO-ESO.

error  $e_{fo}$  and  $e_{ifo}$  with different model parameter  $a_1$  and  $\omega_0$ ,



respectively, when  $a_0 = 10$ . These two figures demonstrate that the mean-square error  $e_{ifo}$  is less prone to the variation of system parameter  $a_1$  and observer parameter  $\omega_0$  than  $e_{fo}$  is. In other words, the IFO-ESO can achieve better estimation performance than FO-ESO.

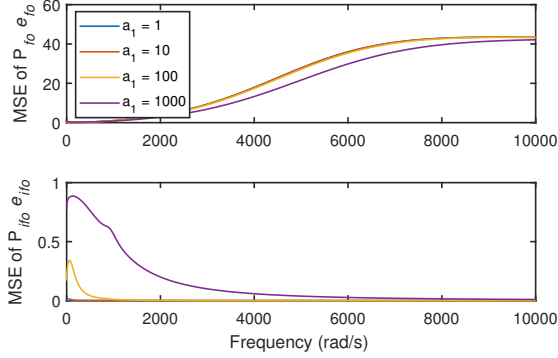


Fig. 4. The MSE curves with different  $a_1$  when  $a_0 = 10$ .

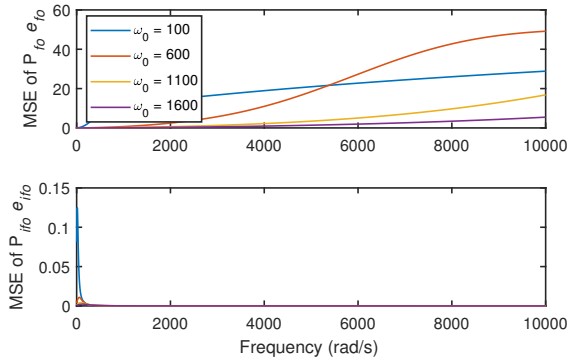


Fig. 5. The MSE curves with different  $\omega_0$  when  $a_0 = 10$ .

## V. TIME-DOMAIN SIMULATION AND COMPARISON

In this section, we will show the performance of the IFO-ADRC in the time-domain using MATLAB/Simulink and compare it with IO-ADRC and FO-ADRC, respectively. The plant used for the simulation is a second-order system (23) where  $a_1 = 10$ ,  $a_0 = 10$ ,  $b_0 = b$ . The structures of IFO-ADRC, FO-ADRC, and IO-ADRC with  $\dot{r} = 0$  and  $\ddot{r} = 0$  are presented in Fig. 1, 6 and 7, respectively. For IFO-ADRC, the observer gains  $L = [\beta_1, \beta_2, \beta_3]^T = [3\omega_0, 3\omega_0^2, \omega_0^3]^T$ ,  $\omega_0 = 1200$ ,  $\gamma = 0.8$ ,  $\nu = 1.2$ , and  $\chi = 1.2$ . The fractional-order operators are discretized by the impulse response invariant method [25] where the discrete frequency for IFO-ESO is 8000 Hz and the discrete order of the fractional-order operators is 6. Note that the observer parameters satisfy conditions of Theorem 3.2, the IFO-ADRC are BIBO stable.

The auxiliary controller  $u_0$  in (14) for IFO-ADRC becomes

$$u_0 = k_{ifp}(r - z_1) - k_{ifd}z_2, \quad (24)$$

TABLE I  
COMPARISON OF THE RESPONSES WITH THREE CONTROL SYSTEMS (SIMULATION)

Controller	Overshoot(%) (K=1.0)	Settling time(s) (K=1.0)	Overshoot fluctuation(%) (K=0.5,1.0,1.5)
IO-ADRC	9.756	0.0833	7.408
IFO-ADRC	9.365	0.0593	0.575

with  $k_p = k_{ifp}$ ,  $k_{d1} = k_{ifd}$ . According to (17), the open-loop transfer function of the IFO-ADRC system can be approximately equivalent to weighted WBTF as follows

$$G_{ifo}(s) = \frac{Z_1(s)}{E_0(s)} \approx \frac{k_{ifp}/k_{ifd}}{s^{1.2}(\frac{1}{k_{ifd}}s^{0.8} + 1)} \quad (25)$$

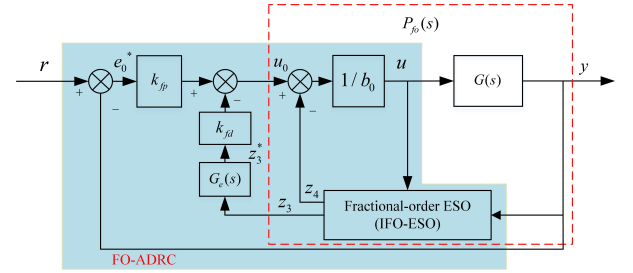


Fig. 6. Structure of the FO-ADRC in [15] for a second-order plant.

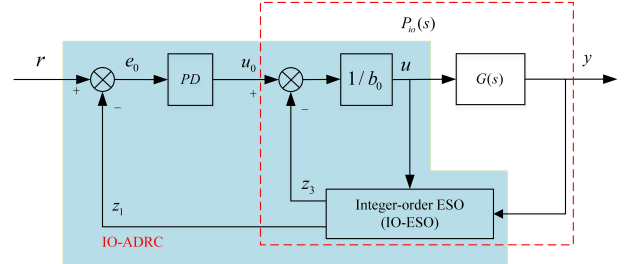


Fig. 7. Structure of the IO-ADRC

### A. Comparison with IO-ADRC

For the fair comparison, let  $k_{ifp}$  and  $k_{ifd}$  in (24) be  $k_{ifp} = 1.2 \times 10^6$  and  $k_{ifd} = 4000$  and the PD controller for IO-ADRC be  $C_{pd}(s) = k_{ip}(1 + k_{id}s)$  with  $k_{ip} = 4466.16$  and  $k_{id} = 0.02562$  such that the open-loop transfer functions of IO-ADRC and IFO-ADRC have the same gain crossover frequency  $\omega_c^* = 114$  rad/s and phase margin  $\varphi_m = 71.3^\circ$ . An external disturbance is imposed for some simulations at 0.3s and lasts until the end of the simulation. The step responses of the IO-ADRC and IFO-ADRC systems are illustrated in Fig. 8, showing that the IFO-ADRC system has better dynamic response performance and disturbance rejection performance than the IO-ADRC system.

Now, let us consider the system performance against controller parameters variation. Multiple the controller parameter  $K_{ifp}$  in the IFO-ADRC system and  $K_{ip}$  in the IO-ADRC

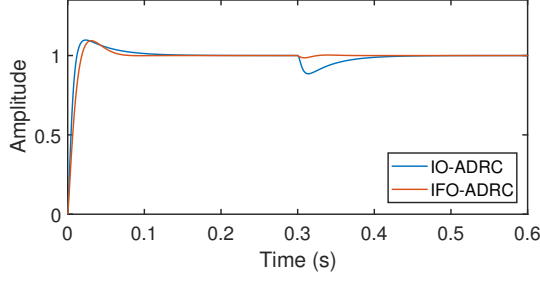


Fig. 8. Step responses of two different control systems

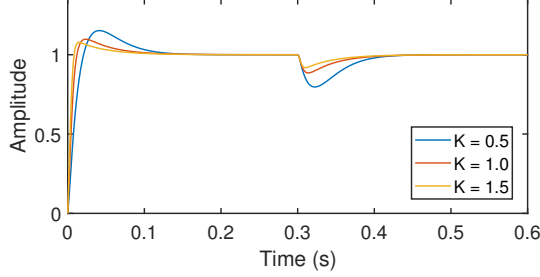


Fig. 9. Step responses of the IO-ADRC control system with controller gain variations

system by  $K$  and consider cases with  $K = 0.5$ ,  $K = 1$  and  $K = 1.5$ . Fig. 9 and Fig. 10 are the step responses of two closed-loop systems when different controller parameters are imposed. As shown in Fig. 10, the IFO-ADRC system are robust to controller gain variations.

When  $K = 0.5$ ,  $K = 1.0$ , or  $K = 1.5$  are set respectively, the maximum speed of the step response are denoted as  $M_K$ . The overshoot fluctuation is calculated as  $\frac{\max\{M_{0.5}, M_{1.0}, M_{1.5}\} - \min\{M_{0.5}, M_{1.0}, M_{1.5}\}}{\text{reference input}}$ . The step responses of two closed-loop systems with different  $K$  are summarized in TABLE I. Note that the overshoots of IFO-ADRC system is smaller than that of the IO-ADRC system. The settling time of the IFO-ADRC system is shorter than the IO-ADRC system.

### B. Comparison with FO-ADRC

For the fair comparison, let  $k_{ifp}$  and  $k_{ifd}$  in (24) be  $k_{ifp} = 9.6 \times 10^4$  and  $k_{ifd} = 400$ , and the parameters of the FO-ADRC be  $k_{fp} = 2.9328 \times 10^5$  and  $k_{fd} = 1222$  (as illustrated in Fig. 6). Let the cut-off frequencies of the two low-pass filters be  $\omega_c^o = 1222$  rad/s. As a result, the open-loop transfer function is approximated as a WBTF

$$G_{fo}(s) \approx \frac{240}{s^{1.2}(\frac{1}{1222}s + 1)} \quad (26)$$

The two WBTFs (25) and (26) have the same gain and cut-off frequencies of the low-pass filters.

The step responses of the FO-ADRC and IFO-ADRC systems are illustrated in Fig. 11 showing that the step response of the IFO-ADRC system has shorter rise time, peak time, and settling time than that of the FO-ADRC system. Multiple the controller parameter  $K_{ifp}$  in the IFO-ADRC system and  $K_{fp}$  in the FO-ADRC system by  $K$  and consider cases with

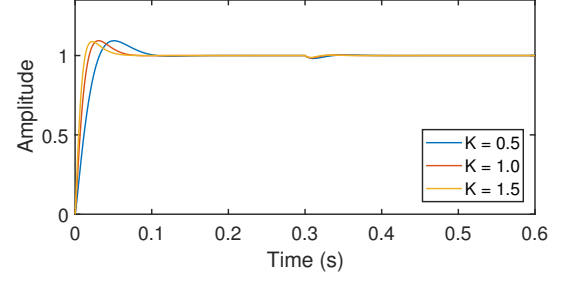


Fig. 10. Step responses of the IFO-ADRC control system with controller gain variations

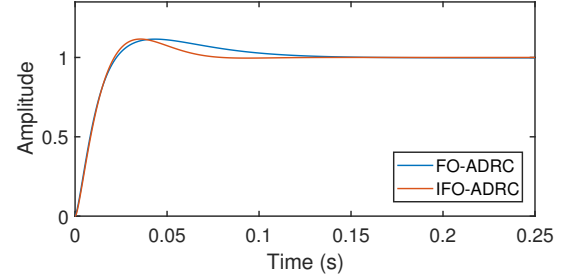


Fig. 11. Step responses of the IFO-ADRC and FO-ADRC systems

TABLE II  
COMPARISON OF THE RESPONSES WITH THE IFO-ADRC AND FO-ADRC SYSTEMS (SIMULATION)

Controller	Overshoot(%) (K=1.0)	Settling time(s) (K=1.0)	Overshoot fluctuation(%) (K=0.8,1.0,1.2)
FO-ADRC	11.551	0.108	1.196
IFO-ADRC	11.591	0.066	0.134

$K = 0.8$ ,  $K = 1$  and  $K = 1.2$ . Fig. 12 and Fig. 13 are the step responses of the IFO-ADRC and FO-ADRC systems when different controller parameters are imposed. It shows the IFO-ADRC system is more robust to controller parameters variations than FO-ADRC system. The step responses of the IFO-ADRC and FO-ADRC with different  $K$  are summarized in TABLE II. It is clearly shown that the settling time of the IFO-ADRC system is shorter than the FO-ADRC system, although the overshoots of IFO-ADRC system is similar to that of the FO-ADRC system.

## VI. EXPERIMENTS: PMSM SPEED SERVO CONTROL

In this section, the performances of IFO-ADRC and IO-ADRC are compared on the PMSM speed servo control system experiments. Fig. 15 is the block diagram of the speed loop of the PMSM speed servo system using IFO-ADRC. In Fig. 15,  $K_1$  is the speed conversion factor,  $T_i$  is the speed feedback filter coefficient, and  $n_r$  is the per unit of the actual speed. The block encircled by the green dash-dotted line in Fig. 15 is the current loop  $G_i(s)$  of the PMSM speed servo system. The PI controller in current loop is designed to ensure that  $G_i(s) = 1$  in the operating frequency band of the speed loop.

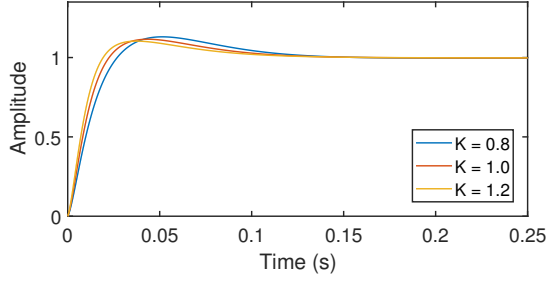


Fig. 12. Step responses of the FO-ADRC systems with controller parameters variations

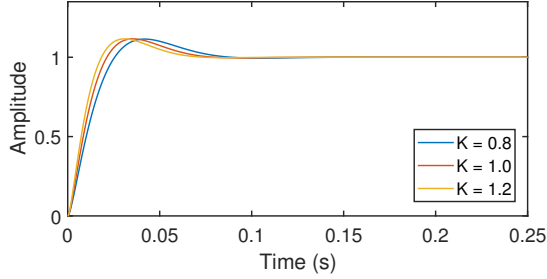


Fig. 13. Step responses of the IFO-ADRC systems with controller parameters variations

The plant of the PMSM speed servo system takes  $i_q$  as the input and  $n_r$  as the output.

The closed-loop controller is implemented on digital signal processor (DSP) illustrated in Fig. 14. The PMSM is 60ST-M00630C and MOSFET is adopted as the gate driver. By system configuration, we set  $K_1 = 1/20000$ ,  $T_i = 1/100$ ,  $K_v = 375\pi C_m/30$ ,  $C_m = 0.112$ ,  $B = 5.747 \times 10^{-4}$  and  $GD^2 = 1.539 \times 10^{-4}$ . The speed sampling period was set as 1 ms, and the current loop sampling period is set as 0.1 ms. The motor speed waveform is collected by DSP Emulator and CCS software. When the specification of the PMSM is used, the plant of the PMSM speed servo system becomes

$$G(s) = \frac{1364.1}{s^2 + 116.4s + 1642}. \quad (27)$$

The same controllers in Section V for IFO-ADRC and IO-ADRC are used. Let the observer gain be  $L = [\beta_1, \beta_2, \beta_3]^T = [3\omega_0, 3\omega_0^2, \omega_0^3]^T$ ,  $\omega_0 = 700$  rad/s,  $b_0 = 1364.1$ ,  $\chi = 1.2$ ,  $\gamma = 0.8$ ,  $\nu = 1.2$ . The fractional-order operators are discretized by the impulse response invariant method [25] where the discrete frequency for IFO-ESO is 1000 Hz and the discrete order of the fractional-order operators is 5. Let  $k_{ifp} = 9000$  and  $k_{ifd} = 300$  for IFO-ADRC,  $k_{ip} = 266.255$  and  $k_{id} = 0.0854$  for IO-ADRC. For each experiment, a constant load torque ( $i_L \approx 0.5$  A) is imposed at 0.75s and lasts until the end of the experiment to mimic the external disturbance.

Fig. 18 compares step responses of the IO-ADRC and IFO-ADRC systems, showing that the step response of the IFO-ADRC system has smaller overshoot, shorter settling time, and smaller speed drop than the IO-ADRC system. Multiple the parameter  $K_{ifp}$  in IFO-ADRC and PD controller parameter  $K_{ip}$  in IO-ADRC by  $K$  and consider  $K = 0.8$ ,  $K = 1$

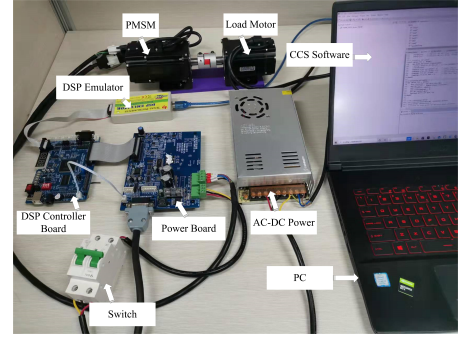


Fig. 14. Experimental platform for control performance validation

and  $K = 1.2$ . Fig. 16 and Fig. 17 are experiment results of step responses with different  $K$  for the IO-ADRC and IFO-ADRC systems, respectively. These two figures show that the IFO-ADRC system is robust to the open-loop gain variations. Table III summarizes results of the step responses for two different systems, showing that the IFO-ADRC system has better performance than the IO-ADRC system.

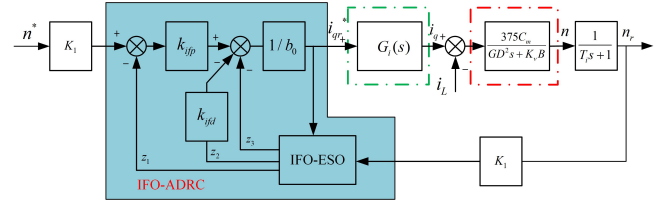


Fig. 15. PMSM speed servo system using IFO-ADRC

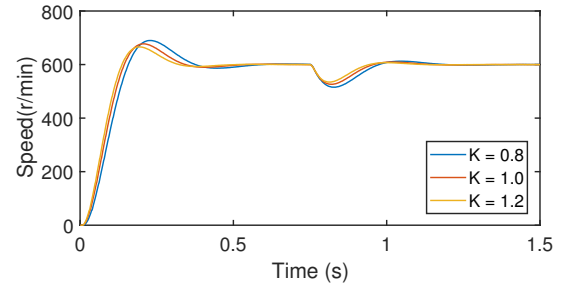


Fig. 16. Step responses of the IO-ADRC with controller gain variations (experiment)

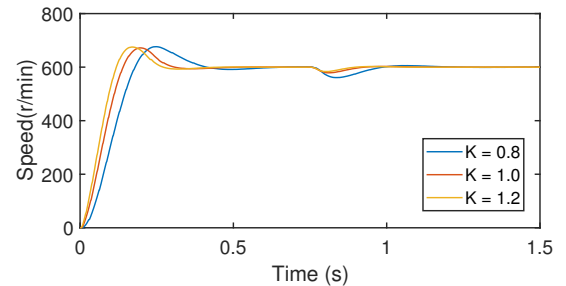


Fig. 17. Step responses of the IFO-ADRC with controller gain variations (experiment)



$$\begin{aligned}
G_m(s) &= \frac{W_1(s)}{E_1(s)} = k_p + \sum_{i=1}^{n-1} k_{d_i} (s^{\chi+(i-1)\gamma} + \sum_{j=1}^{i-1} \beta_j s^{j\gamma} + \beta_i) \\
&\quad + (s^{\chi+(n-1)\gamma} + \sum_{j=1}^{n-1} \beta_j s^{j\gamma} + \beta_n) \\
G_n(s) &= \frac{Y(s)}{W_1(s)} = \frac{1}{s^{\chi+(n-1)\gamma} + \sum_{i=1}^{n-1} k_{d_i} s^{(i-1)\gamma} + k_p}
\end{aligned} \tag{34}$$

where  $W_1(s)$ ,  $Y(s)$  and  $E_1(s)$  are the Laplace transforms of signals  $w_1$ ,  $y$  and  $e_1$ , respectively. According to (31), one has

$$\begin{aligned}
H_m(s) &= \frac{-E_1(s)}{W_2(s)} = \frac{-1}{s^{(n-1)\gamma+\nu+\chi} + \sum_{i=1}^n \beta_i s^{(n-i)\gamma+\nu} + \beta_{n+1}} \\
H_n(s) &= \frac{W_2(s)}{Y(s)} = -s^\nu \sum_{i=0}^{m-1} a_i s^i
\end{aligned} \tag{35}$$

where  $W_2(s)$  is the Laplace transform of signals  $w_2$ .

Now, let us show  $R_2$  is bounded. Let  $d_0 = \sum_{i=0}^m C_{m+1}^i v^{m+1-i} r^{(i)}$  where  $v > 0$  and  $d_1 = k_p r_1 + k_{d_1} r_2 + \dots + k_{d_{n-1}} r_n$ . Define the transfer function of the system as

$$P_1(s) = \frac{D_1(s)}{D_0(s)} = \frac{\sum_{i=1}^{n-1} k_{d_i} s^{\chi+(i-1)\gamma} + k_p}{(s+v)^{m+1}} \tag{36}$$

where  $D_0(s)$  and  $D_1(s)$  are the Laplace transforms of  $d_0$  and  $d_1$ , respectively. The characteristic polynomial of the system  $P_1(s)$  is Hurwitz, i.e., the system  $P_1(s)$  is BIBO stable. As a result,  $\dot{r}, \ddot{r}, \dots, r^{(m-1)}, r^{(m)}$  are bounded, i.e.,  $d_0$  is bounded, then  $d_1$  is bounded. Note that  $R_2 = d_1 + r^{(m)}$ . Since  $r^{(m)}$  is bounded,  $R_2$  is bounded.

Because  $R_1$  and  $R_2$  is bounded, we can treat  $R_1$  and  $R_2$  as the disturbance and calculate the transfer function of the closed-loop system. Further calculation gives

$$G_o(s) = \frac{Y(s)}{E_1(s)} = G_m(s)G_n(s) \tag{37}$$

$$H_o(s) = -\frac{E_1(s)}{Y(s)} = H_m(s)H_n(s) \tag{38}$$

Combining (37) and (38), the transfer function of the closed-loop system  $P_o(s)$  can be given

$$P_o(s) = \frac{Y(s)}{R_o(s)} = \frac{G_o(s)}{1 + G_o(s)H_o(s)} \tag{39}$$

where  $R_o(s)$  is the Laplace transforms of  $r_o$  (see the Fig. 19). Finding positive integers  $p_1, p_2, p_3, q_1, q_2$ , and  $q_3$  such that  $\chi = \frac{p_1}{q_1}$ ,  $\gamma = \frac{p_2}{q_2}$ ,  $\nu = \frac{p_3}{q_3}$ . the characteristic polynomial of the closed-loop system becomes (21). Since  $R_1$  and  $R_2$  is bounded, if the condition of Theorem 3.2 is satisfied, the closed-loop system is BIBO stable [26]. Moreover, the tracking error  $q_1$  converges to a small neighborhood of the origin as  $t \rightarrow \infty$ . ■

**Proof of Theorem 3.3:** When  $m = n = 2$ , the characteristic polynomial of the IFO-ADRC closed-loop system is

$$\begin{aligned}
P(s) &= (s^2 + k_{d_1} s^\chi + k_p)(s^{2\gamma+\chi} + \beta_1 s^2 + \beta_2 s^\gamma + \beta_3) \\
&\quad + (k_p + k_{d_1} s^\chi + \beta_1) + s^2 + \beta_1 s^\gamma + \beta_2)(s^\gamma(a_0 + a_1 s))
\end{aligned}$$

According to Kharitonov-Based Method, since  $\chi = 2 - \gamma$ ,  $0 < \gamma < 1$ ,  $\gamma < \nu < 1$ , when  $\beta_i = C_{n+1}^i \omega_0^i$  for  $i = 1, 2, 3$ , the three boundary polynomials (with (1)  $\gamma = 0, \nu = 0$ ; (2)  $\gamma = 0, \nu = 1$ ; (3)  $\gamma = 1, \nu = 1$ ) can be written

$$\begin{aligned}
{}^1P(s) &= A_0 s^4 + A_1 s^3 + A_2 s^2 + A_3 s + A_4 \\
{}^2P(s) &= B_0 s^5 + B_1 s^4 + B_2 s^3 + B_3 s^2 + B_4 s + B_5 \\
{}^3P(s) &= C_0 s^5 + C_1 s^4 + C_2 s^3 + C_3 s^2 + C_4 s + C_5
\end{aligned} \tag{40}$$

with a list of parameters  $A_i, B_i$  and  $C_i$  for  $i \in \{1, 2, 3, 4, 5\}$ . where

$$\begin{aligned}
A_0 &= 1 + k_{d_1} + 3\omega_0 + 3k_{d_1}\omega_0; A_1 = a_1 + a_1 k_{d_1} \\
A_2 &= a_0 + a_0 k_{d_1} + k_p + 3k_p\omega_0 + 3\omega_0^2 + 3k_{d_1}\omega_0^2 + \omega_0^3 \\
&\quad + k_{d_1}\omega_0^3 \\
A_3 &= a_1 k_p + 3a_1\omega_0 + 3a_1 k_{d_1}\omega_0 + 3a_1\omega_0^2 \\
A_4 &= a_0 k_p + 3a_0\omega_0 + 3a_0 k_{d_1}\omega_0 + 3a_0\omega_0^2 + 3k_p\omega_0^2 + k_p\omega_0^3 \\
B_0 &= 1 + k_{d_1}; B_1 = a_1 + a_1 k_{d_1} + 3\omega_0 + 3k_{d_1}\omega_0 \\
B_2 &= a_0 + a_0 k_{d_1} + k_p + 3\omega_0^2 + 3k_{d_1}\omega_0^2 \\
B_3 &= a_1 k_p + 3a_1\omega_0 + 3a_1 k_{d_1}\omega_0 + 3k_p\omega_0 + 3a_1\omega_0^2 + \omega_0^3 \\
&\quad + k_{d_1}\omega_0^3 \\
B_4 &= a_0 k_p + 3a_0\omega_0 + 3a_0 k_{d_1}\omega_0 + 3a_0\omega_0^2 + 3k_p\omega_0^2 \\
B_5 &= k_p\omega_0^3; C_0 = 1; C_1 = a_1 + k_{d_1} + 3\omega_0 \\
C_2 &= a_0 + a_1 k_{d_1} + k_p + 3a_1\omega_0 + 3k_{d_1}\omega_0 + 3\omega_0^2 \\
C_3 &= a_0 k_{d_1} + a_1 k_p + 3a_0\omega_0 + 3a_1 k_{d_1}\omega_0 + 3k_p\omega_0 + 3a_1\omega_0^2 \\
&\quad + 3k_{d_1}\omega_0^2 + \omega_0^3 \\
C_4 &= a_0 k_p + 3a_0 k_{d_1}\omega_0 + 3a_0\omega_0^2 + 3k_p\omega_0^2 + k_{d_1}\omega_0^3 \\
C_5 &= k_p\omega_0^3
\end{aligned} \tag{41}$$

Firstly, we consider  ${}^1P(s) = 0$ . When  $a_1 \geq 0, a_0 \geq 0, k_p > 0$ , and  $\omega_0 > 0$ , from (41), we have  $A_0 > 0, A_1 \geq 0$ , and  $A_2 > 0$ . When  $k_{d_1} > 8$  and  $\omega_0$  is sufficiently large,  $A_1 A_2 > A_3 A_4$  and  $A_1 A_2 A_3 > A_0 A_3^2 + A_1^2 A_4$ . According to Routh-Hurwitz criterion, all the roots of  ${}^1P(s) = 0$  are located in left plane, i.e., when  $a_1 \geq 0, a_0 \geq 0$  and  $k_{d_1} > 8$ , there exists a sufficiently large  $\omega_0 > 0$ , such that all the root of  ${}^1P(s) = 0$  are located in left plane.

TABLE IV  
ROUTH TABLE OF  ${}^2P(s) = 0$

$s^5$	$B_0$	$B_2$	$B_4$
$s^4$	$B_1$	$B_3$	$B_5$
$s^3$	$D_1$	$D_5$	
$s^2$	$D_2$	$D_6$	
$s^1$	$D_3$		
$s^0$	$D_4$		

Secondly, we consider  ${}^2P(s) = 0$ . According to Routh-Hurwitz criterion,  ${}^2P(s) = 0$  can be written as the Routh

table form as TABLE IV. In TABLE IV,  $C_1$ ,  $C_2$ ,  $C_3$ , and  $C_4$  are

$$C_1 = \frac{N_5}{D_5}, C_2 = \frac{N_6}{D_6}, C_3 = \frac{N_7}{D_7}, C_4 = k_p \omega_o^3 \quad (42)$$

where

$$\begin{aligned} N_5 &= a_0 a_1 + 3a_1^2 \omega_o + 9a_1 \omega_o^2 + 8\omega_o^3, D_5 = a_1 + 3\omega_o \\ N_6 &= 3a_1(a_0^2 + a_1^2 k_p) \omega_o + (9a_0 a_1^2 + 15a_1^2 k_p) \omega_o^2 \\ &\quad + a_1(10a_0 + 9a_1^2 + 18k_p) \omega_o^3 + 30a_1^2 \omega_o^4 + 33a_1 \omega_o^5 \\ &\quad + 8\omega_o^6 - 3a_1 a_0 k_p - 9a_0 k_p - 3a_0 \omega_o^4 \\ D_6 &= a_0 a_1 + 3a_1^2 \omega_o + 9a_1 \omega_o^2 + 8\omega_o^3 \\ N_7 &= 3(a_0^3 a_1 k_p + a_0 a_1^3 k_p^2) + (9a_0^2 a_1^2 k_p \\ &\quad + 15a_0 a_1^2 k_p^2) \omega_o + (9a_0^3 a_1 + 9a_0^2 a_1 k_p \\ &\quad + 18a_0 a_1^3 k_p + 9a_0 a_1 k_p^2 + 9a_1^3 k_p^2) \omega_o^2 + (27a_0^2 a_1^2 \\ &\quad + 96a_0 a_1^2 k_p - 24a_0 k_p^2 + 42a_1^2 k_p^2) \omega_o^3 + (30a_0^2 a_1 \\ &\quad + 27a_0 a_1^3 + 108a_0 a_1 k_p + 18a_1^3 k_p + 48a_1 k_p^2) \omega_o^4 \\ &\quad + (90a_0 a_1^2 + 54a_1^2 k_p) \omega_o^5 + (99a_0 a_1 + 48a_1 k_p) \omega_o^6 \\ &\quad + 24a_0 \omega_o^7 - 3a_0^2 a_1 k_p^2 - 9a_0^2 k_p^2 \omega_o - 30a_0^2 k_p \omega_o^3 \\ &\quad - 9a_0^2 \omega_o^5 \\ D_7 &= 3a_1(a_0^2 + a_1^2 k_p) + (9a_0 a_1^2 + 15a_1^2 k_p) \omega_o \\ &\quad + a_1(10a_0 + 9a_1^2 + 18k_p) \omega_o^2 + 30a_1^2 \omega_o^3 + 33a_1 \omega_o^4 \\ &\quad + 8\omega_o^5 - 3a_1 a_0 k_p - 9a_0 k_p \omega_o - 3a_0 \omega_o^3 \end{aligned} \quad (43)$$

When  $a_0 \geq 0$ ,  $a_1 \geq 0$ , and  $\omega_o$  is sufficiently large, we have  $B_0 > 0$ ,  $B_1 > 0$ ,  $C_1 > 0$ ,  $C_2 > 0$ ,  $C_3 > 0$ , and  $C_4 > 0$ . According to Routh-Hurwitz criterion, if  $B_0 > 0$ ,  $B_1 > 0$ ,  $C_1 > 0$ ,  $C_2 > 0$ ,  $C_3 \geq 0$ , and  $C_4 > 0$ , then all the roots of  ${}^2P(s) = 0$  are located in the left plane. Similar to the determination of the location of the root of  ${}^2P(s) = 0$ , when  $a_0 \geq 0$ ,  $a_1 \geq 0$ , and  $\omega_o$  is sufficiently large, all the roots of  ${}^3P(s) = 0$  are located in the left plane. According to Kharitonov-Based Method, when the three boundary polynomials are stable, the closed-loop system is BIBO stable, ie., when  $\gamma < \nu < 1$ ,  $m = n = 2$ ,  $a_1 \geq 0$ ,  $a_0 \geq 0$ ,  $k_{d1} > 8$  and  $\beta_i = C_{n+1}^i \omega_o^i$  for  $i = 1, 2, 3$ , there always exists a constant  $\omega_o > 0$ , such that the closed-loop system is BIBO stable. ■

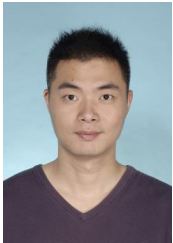
## REFERENCES

- [1] L. Liu, H. Xing, X. Cao, Z. Fu, and S. Song, "Guaranteed cost finite-time control of discrete-time positive impulsive switched systems," *Complexity*, vol. 2018, 2018.
- [2] Y.-F. Pu, Z. Yi, and J.-L. Zhou, "Fractional hopfield neural networks: Fractional dynamic associative recurrent neural networks," *IEEE transactions on neural networks and learning systems*, vol. 28, no. 10, pp. 2319–2333, 2016.
- [3] G. Tzounas, I. Dassios, M. A. A. Murad, and F. Milano, "Theory and implementation of fractional order controllers for power system applications," *IEEE Transactions on Power Systems*, vol. 35, no. 6, pp. 4622–4631, 2020.
- [4] F. M. Zaihidee, S. Mekhilef, and M. Mubin, "Application of fractional order sliding mode control for speed control of permanent magnet synchronous motor," *IEEE Access*, vol. 7, pp. 101 765–101 774, 2019.
- [5] A. Gomaa Haroun and L. Yin-Ya, "A novel optimized fractional-order hybrid fuzzy intelligent PID controller for interconnected realistic power systems," *Transactions of the Institute of Measurement and Control*, vol. 41, no. 11, pp. 3065–3080, 2019.
- [6] H. Li, Y. Luo, and Y. Chen, "A fractional order proportional and derivative (FOPD) motion controller: tuning rule and experiments," *IEEE Transactions on control systems technology*, vol. 18, no. 2, pp. 516–520, 2009.
- [7] D. Li, P. Ding, and Z. Gao, "Fractional active disturbance rejection control," *ISA transactions*, vol. 62, pp. 109–119, 2016.
- [8] H. W. Bode et al., "Network analysis and feedback amplifier design," 1945.
- [9] W. Zheng, Y. Luo, Y. Chen, and X. Wang, "Synthesis of fractional order robust controller based on bode's ideas," *ISA transactions*, vol. 111, pp. 290–301, 2021.
- [10] N. Zhuo-Yun, Z. Yi-Min, W. Qing-Guo, L. Rui-Juan, and X. Lei-Jun, "Fractional-order pid controller design for time-delay systems based on modified bode's ideal transfer function," *IEEE Access*, vol. 8, pp. 103 500–103 510, 2020.
- [11] R. S. Barbosa, J. T. Machado, and I. M. Ferreira, "Tuning of pid controllers based on bode's ideal transfer function," *Nonlinear dynamics*, vol. 38, no. 1, pp. 305–321, 2004.
- [12] S. P. Jadhav, S. T. Hamde et al., "Robust fractional-order controller using bode's ideal transfer function for power plant gas turbine," *International Journal of Computer Applications*, vol. 88, no. 16, pp. 1–7, 2014.
- [13] D. S. Patil, M. D. Patil, and V. A. Vyawahare, "Design of fractional-order controller for fractional-order systems using bode's ideal loop transfer function method," in *2015 International Conference on Industrial Instrumentation and Control (ICIC)*. IEEE, 2015, pp. 490–495.
- [14] Y.-B. Zhang and Y.-G. Pi, "Fractional order controller for pmsm speed servo system based on bode's ideal transfer function," *Sensors & Transducers*, vol. 173, no. 6, p. 110, 2014.
- [15] U. M. Al-Saggaf, R. Mansouri, M. Bettayeb, I. M. Mehedi, and K. Munawar, "Robustness improvement of the fractional-order ladc scheme for integer high-order system," *IEEE Transactions on Industrial Electronics*, vol. 68, no. 9, pp. 8572–8581, 2020.
- [16] Z. Gao, "Scaling and bandwidth-parameterization based controller tuning," in *Proceedings of the American control conference*, vol. 6, 2006, pp. 4989–4996.
- [17] M. Ran, J. Li, and L. Xie, "A new extended state observer for uncertain nonlinear systems," *Automatica*, vol. 131, p. 109772, 2021.
- [18] H. Feng and S. Li, "Active disturbance rejection control based on weighed-moving-average-state-observer," *Journal of Mathematical Analysis and Applications*, vol. 411, no. 1, pp. 354–361, 2014.
- [19] H. L. Serrano, I. Chairez, and A. Luviano-Juárez, "Composite active disturbance rejection robust control for a prototype of an active damping artificial ankle prosthesis," *Asian Journal of Control*, vol. 22, no. 2, pp. 908–923, 2020.
- [20] Z. Chen and D. Xu, "Output regulation and active disturbance rejection control: unified formulation and comparison," *Asian Journal of Control*, vol. 18, no. 5, pp. 1668–1678, 2016.
- [21] G. S. Teodoro, J. T. Machado, and E. C. De Oliveira, "A review of definitions of fractional derivatives and other operators," *Journal of Computational Physics*, vol. 388, pp. 195–208, 2019.
- [22] E. Yumuk, M. Güzelkaya, and İ. Eksin, "Analytical fractional pid controller design based on bode's ideal transfer function plus time delay," *ISA transactions*, vol. 91, pp. 196–206, 2019.
- [23] W. Deng, C. Li, and J. Lü, "Stability analysis of linear fractional differential system with multiple time delays," *Nonlinear Dynamics*, vol. 48, no. 4, pp. 409–416, 2007.
- [24] M. H. Richardson and D. L. Formenti, "Parameter estimation from frequency response measurements using rational fraction polynomials," in *Proceedings of the 1st international modal analysis conference*, vol. 1. Union College Schenectady, NY, 1982, pp. 167–186.
- [25] Y. Chen, "Impulse response invariant discretization of fractional order integrators/differentiators," May 2009, uRL <http://www.mathworks.com/matlabcentral/leexchange/21342impulseresponse-invariant-discretization-of-fractional-orderintegrators-differentiator>.
- [26] I. Petráš, *Fractional-order nonlinear systems: modeling, analysis and simulation*. Springer Science & Business Media, 2011.
- [27] I. Petráš, Y. Chen, and B. M. Vinagre, "A robust stability test procedure for a class of uncertain lti fractional order systems," in *Proc. of ICCCT2002*, May, 2002, pp. 27–30.





**Bolin Li** received the M.E. degree in Mechanical and Electronic Engineering from Huazhong University of Science and Technology, Wuhan, China, in 2021. He is currently pursuing the Ph.D. degree in School of Artificial Intelligence and Automation, the Huazhong University of Science and Technology (HUST), Wuhan, China. His research mainly involves active disturbance rejection control and fractional-order PID control.



**Lijun Zhu** received the Ph.D. degree in Electrical Engineering from University of Newcastle, Callaghan, Australia, in 2013. He is now a Professor in the School of Artificial Intelligence and Automation, Huazhong University of Science and Technology, Wuhan, China. His research interests include robotics, nonlinear systems analysis and control.